Chemical Engineering Science 257 (2022) 117693

Contents lists available at ScienceDirect

Chemical Engineering Science

journal homepage: www.elsevier.com/locate/ces

# Oxygen transfer of microbubble clouds in aqueous solutions – Application to wastewater

Thomas Abadie [a,b], Sultan M. al Ma Awali [a,b], Brian Brennan [a,d,c], Ciprian Briciu-Burghina [a,d], Mohammad Tajparast [a,c], Thayse Marques Passos [a,c], John Durkan [e], Linda Holland [a,c], Jenny Lawler [a,c], Kieran Nolan [a,d], Brid Quilty [a,c], Lorna Fitzsimons [a,b], Fiona Regan [a,d,*], Yan Delauré [a,b,*]

[a] Water Institute, Dublin City University, Glasnevin, Dublin, Ireland
[b] School of Mechanical and Manufacturing Engineering, Dublin City University, Glasnevin, Dublin, Ireland
[c] School of Biotechnology, Dublin City University, Glasnevin, Dublin, Ireland
[d] School of Chemical Sciences, Dublin City University, Glasnevin, Dublin, Ireland
[e] ABP Food Group, Cahir, Co., Tipperary, Ireland

## HIGHLIGHTS

- Lab experiments are compared to industrial wastewater with microbiological activity.
- Triton X100 and wastewater are shown to hamper oxygen transfer similarly.
- OTE is enhanced with microbubbles and decreases as the injection rate increases.
- The contributions to oxygen transfer are studied through dual measurements.
- The effects of contaminants on mass transfer weaken as the bubble sizes and Re increase.

## ARTICLE INFO

*Article history:*
Received 2 January 2022
Received in revised form 11 April 2022
Accepted 22 April 2022
Available online 11 May 2022

*Keywords:*
Microbubbles
Bubble column
Oxygen transfer
Surfactants
Wastewater

## ABSTRACT

This study aims at improving the knowledge on the effects of gas injection, bubbles sizes and contaminants on oxygen transfer in microbubble clouds. First the effects of gas injection on oxygen transfer are studied and linked to several parameters that change together with changes in flow rate, namely bubble sizes and rise velocities. Oxygen transfer is then studied in the presence of contaminants that are shown to affect bubble size distribution, modify bubble dynamics and interfacial mass transfer. Oxygen transfer efficiencies are also measured in wastewater and compared with those obtained in aqueous solutions. The agreement between contaminated water in the lab (Triton X100) and wastewater experiments is emphasised as this offers the possibility to develop fundamental understanding relevant to wastewater under laboratory conditions. The role of the surfactants on the volumetric oxygen transfer coefficient is further analysed in terms of specific interfacial area and transfer coefficients, respectively. Interestingly, this shows that the increase in oxygen transfer efficiency as the concentration in Pentanol increases is due to the increase in interfacial area while the transfer coefficients decrease.


## 1. Introduction

Bubbly flows are widely used in industrial and environmental applications for their mixing and transfer properties. Bubbles and fine bubbles specifically have been found to provide a number of benefits for various applications such as water treatment bioreactors (Garcia-Ochoa and Gomez, 2009; Durán et al., 2016), activated sludge (Terasaka et al., 2011), removal of fine particles (Rubio et al., 2002; Rodrigues and Rubio, 2007) as well as defouling of solid surfaces (Wu et al., 2008) or decontamination (Khadre et al., 2001). Reducing bubble sizes allow for enhanced surface to volume ratio. This key characteristic has made the study of microbubbles a key research topic over the past few years and their interesting properties -*e.g.* enhanced residence time, high interfacial areas, interface charge- have been reviewed recently (Takahashi, 2005; Agarwal et al., 2011; Khuntia et al., 2012; Parmar and Majumder, 2013; Tsuge, 2014).

Although the generation of a small number of microbubbles can be achieved with a fine control in microfluidic devices, high

* Corresponding authors.
*E-mail addresses:* fiona.regan@dcu.ie (F. Regan), yan.delaure@dcu.ie (Y. Delauré).

https://doi.org/10.1016/j.ces.2022.117693
0009-2509/

throughputs remain a challenge (Rodríguez-Rodríguez et al., 2015). The generation of microbubbles for industrial applications with large production rates and a fine control on bubble sizes is therefore still investigated extensively through a number of methods. While membranes or perforated plates are commonly used in industrial aeration tanks, Zimmerman et al. (2011), Tesar (2013), Tesar (2014), Tesar and Peszynski (2014), Brittle et al. (2015) devised a fluidic oscillator to minimise the bubble sizes and maximise the production rate in porous diffusers. A number of authors use mixers where the gaseous phase is introduced in rotating flows and breaks in small bubbles due to turbulence effects (Kawahara et al., 2009; Li and Tsuge, 2006). A popular technique in Dissolved Air Floatation systems uses hydrodynamic cavitation where pressurised water saturated in air flows through an orifice leading to a sudden depressurisation. The dissolved gases concentrations (including oxygen and nitrogen) exceed the saturation levels that decreased with the drop in pressure, thereby generating microbubbles (Rodrigues and Rubio, 2007; Zhang et al., 2015). Two-phase pumps are also used to combine the two latter generation mechanisms: the rotating flows allow to enhance the dissolution of oxygen into the continuous phase and the depressurised flow leads to bubble generation through hydrodynamic cavitation (Etchepare et al., 2017; Muroyama et al., 2013).

The use of microbubbles and nanobubbles for improved floatation is also widely discussed in recent literature (Rubio et al., 2002; Rodrigues and Rubio, 2007; Calgaroto et al., 2014; Calgaroto et al., 2015; Etchepare et al., 2017), while their aeration properties have been discussed more scarcely in the literature (Terasaka et al., 2011; Muroyama et al., 2012; Muroyama et al., 2013; Liu et al., 2018). At the scale of a bubble, extensive studies on mass transfer have been performed theoretically (Brenner, 1963), experimentally (Takemura and Yabe, 1998), as well as numerically (Figueroa-Espinoza and Legendre, 2010) and the Sherwood number has been correlated to the Reynolds and Peclet numbers from diffusive to convective regimes. More recently, the effects of the shape of bubbles on mass transfer have been investigated numerically (Figueroa-Espinoza and Legendre, 2010). A number of studies considered the collective effects in a bubble swarm on mass transfer and it was shown that transfer rates and drag coefficients are slightly enhanced when compared to single bubble correlations (Colombet et al., 2011; Colombet et al., 2015; Roghair et al., 2016). Colombet et al. (2015) suggested through dimensional analysis that the void fraction has nearly negligible effects in their experiments due to the high Peclet number ($> 10^5$) and therefore the boundary layer is very thin when compared with the distance between bubbles and the turbulent eddies. In large tanks, millimetric bubbles are often preferred to enhance mass transfer thanks to improved convection around the interface but their residence time can be a limiting factor. Muroyama et al. (2013) conducted an interesting study on mass transfer in microbubble clouds and showed transfer efficiencies that can reach above 80–100% in a microbubble cloud in a water depth of 1 m. Similar findings were presented in Terasaka et al. (2011) where various bubbles generators were investigated. However, although faster absorption rates can be achieved with reduced bubble sizes it was shown that the power consumption to break bubbles into micro or nanobubbles is also increased significantly. A trade off between power consumption, costs and absorption rates therefore needs to be achieved.

In addition, most of those studies were conducted in pure or tap water and the effects of surfactants on mass transfer coefficients are often overlooked. Alpha factors which measure the ratio of transfer efficiency in presence of surfactants with the transfer efficiency in clean water have been measured (Rosso et al., 2006; Rosso and Stenstrom, 2006, Germain et al., 2007). McClure et al. (2017) showed a decrease in the Oxygen Transfer Rate in a bubble column when increasing the concentration of antifoaming agents until a threshold where the interfacial area is completely covered by a monolayer of antifoaming agents. However, only overall quantities (transfer efficiency, volumetric mass transfer coefficient) are analysed and their link to the bubble size or dynamics is not provided. Vasconcelos et al. (2003) showed a decrease in mass transfer coefficients in millimetric bubble swarms with surfactant concentration. They correlated their results through the increase in drag as the interface rigidifies.

On the other hand, the effects of surfactants on mass transfer around millimetric bubble trains with frequencies ranging from 5 to 30 bubbles per second have been studied by Sardeing et al. (2006), Hebrard et al. (2009). Jimenez et al. (2014) recently presented mass transfer coefficients through visualisation techniques. Results were reported for a clean interface rising in stagnant liquid and for a contaminated bubble in a Hele-Shaw cell. The resulting mass transfer coefficient was found to be lower than the one for a rigid sphere while the rigid sphere asymptotic case was found to be the lower value for the mass transfer coefficient of contaminated bubbles in earlier studies (Vasconcelos et al., 2003). This is of particular interest as it shows that the liquid side mass transfer reduction in the presence of surfactants is not only due to a change in dynamics (bubble rise velocity), but also because surfactants act as a "barrier to mass transfer". Lebrun et al. (2022) recently investigated the effects of the nature of surfactants, *i.e.* cationic surfactants with varying hydrophobic chain lengths and nonionic surfactants with varying hydrophylic chain lengths, on mass transfer coefficients for millimetric bubbles. For a given bulk concentration of surfactants, it was shown that mass transfer coefficients were reduced when increasing the hydrophobic chain length of surfactants.

The present paper focuses on microbubble clouds with Sauter diameters in the range 100–3000$\mu$m as they are considered to be a good trade-off between bubbles of 1–10$\mu$m diameter and millimetric ones in terms of mass transfer. The first part aims at describing the experimental methodologies, both in the lab with aqueous solutions and on site with wastewater. After describing the methodology, the effects of operating conditions and contamination are analysed with regard to bubble sizes, dynamics and oxygen transfer rates. The oxygen transfer efficiencies are compared to the results obtained with wastewater to show the efficiency of microbubble clouds and the effects of the operating conditions (gas superficial velocity) on transfer efficiencies. In addition, the results obtained with Triton X100 are of particular interest as they are shown to agree very well with oxygen transfer results obtained in wastewater while being performed under laboratory conditions with access to visualisation equipment and a finer control of operating conditions. This is in agreement with the work of McClure et al. (2014) who observed that the use of aqueous solutions of 2-propanol yields to a similar behaviour to the fermentation media used in aerobic processes and can therefore be used as "a meaningful physical analogue in pilot-scale experimentation". Finally, the effects of interface contamination in aqueous solutions of Pentanol and Triton X100 on global volumetric mass transfer coefficients $k_La$ are investigated by splitting their effects in two contributions, namely the interfacial area and the mass transfer coefficient $k_L$.

## 2. Methodology

### 2.1. Experimental set-up with aqueous solutions

#### 2.1.1. Bubble column and microbubble injection

Microbubble clouds are generated with compressed gas through a ceramic plate (Pentair MBD100 - $30.8 \times 2.86$ cm$^2$),

which sits at the bottom of a column of dimensions $1.20 \times 0.50 \times 0.10$ m$^3$ (see Fig. 1). Nitrogen is used to deoxygenate the water at the beginning of the experiments (Colombet et al., 2013; Muroyama et al., 2013) and the flow is switched to compressed air when the dissolved oxygen level reaches values lower than 5% of the oxygen saturation in water, *i.e.* about 0.45 mg/L. The gauge pressure is measured in the feed line with a pressure sensor (ABB 261 for pressures in the range from $-1$ to 10 bars) and set with a manual valve while the flow rate is measured with a thermal mass flow meter (Sierra SmartTrak 50 for flow rates in the range 0–50 NL/min).

### 2.1.2. Choice of contaminants

The effects of contaminants on bubble dynamics and mass transfer are of key importance for practical application, such as wastewater treatment. Surfactants have been chosen in agreement with those used in Takagi and Matsumoto (2011), *i.e.* Triton X100 and Pentanol-3. In their work, it is shown that bubbles in aqueous solutions of Triton X100 behave like solid spheres with no-slip at the interface, even at low concentration (*e.g.* $C = 0.0007\, mol \cdot m^{-3}$). On the other hand, bubbles in aqueous solutions of Pentanol-3 behave like water at low concentrations ($C = 0.037\, mol \cdot m^{-3}$) and tend towards solid spheres dynamics as the concentration increases ($C = 1.39\, mol \cdot m^{-3}$). The Langmuir adsorption model is used to estimate the surface concentration as a function of the concentration in the bulk and the ratio of adsorption to desorption rates:

$$\Gamma = \Gamma_{max} \frac{K_{LG} C_\infty}{1 + K_{LG} C_\infty}, \tag{1}$$

where $\Gamma$ is the surfactant concentration at the interface, $\Gamma_{max}$ the maximum surface concentration, $K_{LG}$ the Langmuir constant and $C_\infty$ the concentration of surfactant in the bulk. The parameters of the two aqueous solutions of Triton X100 and five aqueous solutions of Pentanol-3 used to investigate the effects of contaminants on bubbles sizes and mass transfer are reported in Table 1. The Langmuir coefficient being much larger for Triton X100 than Pentanol-3, the coverage dynamics is expected to happen at lower concentrations in Triton X100. It should also be noted that as the bubbles are rising, the surfactants are transported to the rear of the bubble. The surface concentration at the front of the bubble thus decreases below the equilibrium value and surfactants keep being adsorbed at the front while being desorbed at the rear. This renewal of the interface can lead to average surface concentrations above the equilibrium one at low bulk concentration and Reynolds numbers above 20 (Takemura, 2005). However, this model does not account for the number of bubbles or the total interfacial area. McClure et al. (2017) used as reference the concentration for monolayer coverage $C_{monolayer} = aM_w\Gamma_{max}/\rho$ with $M_w$ and $\rho$ being the molar mass and the density of the surfactant. Considering the maximum volumetric interfacial area in our experiments ($70m^{-1}$), this expression leads to monolayer concentrations of c. $4.5 \times 10^{-8} mol.m^{-3}$ for Pentanol-3 and $10^{-7} mol.m^{-3}$ for Triton X100. This indicates that the surfactant coverage is not limited by the bulk concentration but by the adsorption/desorption kinetics at the interface in our experiments.

### 2.1.3. Bubbles visualisation and tracking

Bubble sizes and velocities are estimated through shadow tracking with a camera DANTEC (FlowSense EO4M, with up to 41 Hz sampling rate and sensor resolution 2336 px $\times$ 1752 px) mounted with a lens with a magnification ratio 2.2. Due to the low sampling rate, pairs of images are acquired in double frame mode with a time shift of 0.5–1 ms to calculate the bubble velocities with a frequency of 1 Hz to 10 Hz. In double frame mode, the exposure time can however not be set and a dual laser (DANTEC DualPower 65–15 - 532 nm wave length, 62 mJ pulse energy, 4 mm beam, 2.5mrad divergence and up to 15 Hz frequency) is synchronised with the camera for illumination. The dual laser is used together with a light guide and a lens (DANTEC Shadow Strobe[1]) as light source in order to provide a very uniform and bright background during a very short time, thereby "freezing" the motion of bubbles. The images acquired are processed with the visualisation toolbox of MATLAB. Thresholding on the gray levels and gradients is used to detect the contours of bubbles, relying on the built-in watershed algorithm to separate bubbles. Bubbles are tracked according to several criteria such as the size, shape and minimum displacement. An example of images obtained and the contours and center of mass of the bubbles detected is shown in Fig. 2. From the image processing analysis, the bubble sizes as well as their minimum and maximum axes ($m_i$ and $l_i$) if they are not spherical are evaluated. The Sauter diameter, which corresponds to the diameter of a bubble with an equivalent volume to surface ratio and which is well suited to compare polydisperse and monodisperse systems as suggested by Tavassoli et al. (2017), is estimated as:

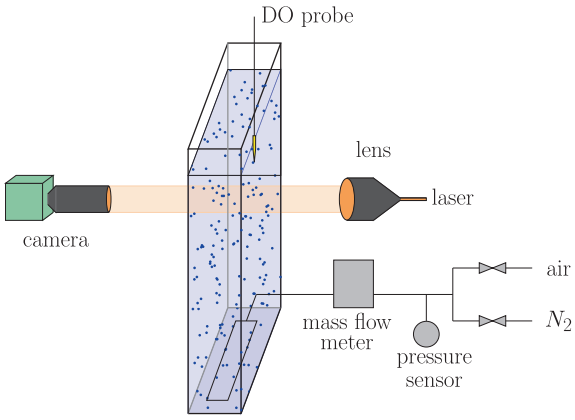


**Fig. 1.** Schematic of the experimental rig with sensing equipment -mass flow rate, pressure, dissolved oxygen- and visualisation one -camera, laser-.

$$d_{sa} = \frac{\sum_i d_{vi}^3}{\sum_i d_{si}^2}, \tag{2}$$

where $d_{vi}$ and $d_{si}$ are the equivalent diameters of a spherical bubble with the same volume and surface area respectively. Considering the bubbles are oblate spheroids, $d_{vi}$ and $d_{si}$ are defined as (Weisstein, 2003; Muroyama et al., 2013):

$$d_{vi} = \sqrt[3]{l_i^2 m_i} \tag{3}$$

$$d_{si} = \begin{cases} l_i & \text{if} \quad (l_i - m_i)/l_i < 0.01, \\ \sqrt{\frac{1}{2} l_i^2 \left[ 1 + \frac{m_i^2}{l_i \sqrt{l_i^2 - m_i^2}} \ln\left( \frac{l_i + \sqrt{l_i^2 - m_i^2}}{m_i} \right) \right]} & \text{otherwise.} \end{cases} \tag{4}$$

The Sauter diameter of a single bubble and the specific interfacial area are defined as:

[1] https://www.dantecdynamics.com/wp-content/uploads/2021/09/0520_v3_SS_Shadow-Sizing.pdf.

**Table 1**
Adsorption parameters and surfactant concentrations. The values are adapted from Lebrun et al. (2022) for Triton X100 and Matsumoto et al. (2006) for Pentanol-3. Note that Matsumoto et al. (2006) reported values for Pentanol-1 but Walz et al. (2016) showed that the Langmuir constant is similar for Pentanol-3 and Pentanol-1.

| | Triton X100 | | | | Pentanol-3 | | |
|---|---|---|---|---|---|---|---|
| $\Gamma_{max}\,[mol \cdot m^{-2}]$ | $2.67 \times 10^{-6}$ | | | | $5.9 \times 10^{-6}$ | | |
| $K_{LG}\,[m^3 \cdot mol^{-1}]$ | 1053 | | | | $4.6 \times 10^{-2}$ | | |
| $C_\infty\,[mol \cdot m^{-3}]$ | 0.00071 | 0.00147 | 0.037 | 0.1 | 0.2 | 0.4 | 1.39 |
| $\Gamma/\Gamma_{max}[\times 10^{-2}]$ | 42.8 | 60.8 | 0.170 | 0.458 | 0.912 | 1.81 | 6.01 |

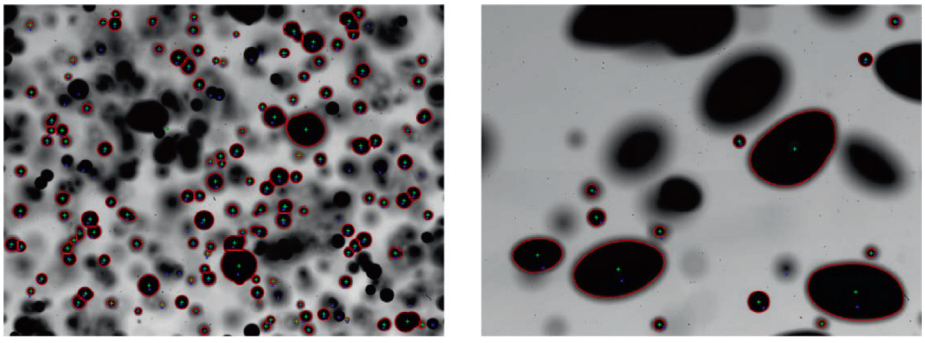

(a) $Q_G = 0.41L/min$ (b) $Q_G = 4.67L/min$

**Fig. 2.** Examples of images processed for two different flow rates of air and presenting different bubble sizes ranges. The red lines show the contours of the bubbles detected, the green crosses show their center of mass and the blue ones show the center of mass of bubbles detected in the previous image. The region of interest corresponds to an area $15 \times 15mm^2$.

$$d_{sa,i} = \frac{d_{vi}^3}{d_{si}^2}, \tag{5}$$

$$a = \frac{\sum a_i}{V_{tot}}, \tag{6}$$

where $a_i = \pi d_{sa,i}^2$ is the interfacial area of each single bubble and $V_{tot}$ is the total volume of the bubble column.

*2.1.4. Oxygen transfer*

In order to study oxygen transfer in aqueous solution, dissolved oxygen (DO) concentration in water is measured with an optical DO probe Presens microsensor (NTH-Pst1) with a response time less than 5s with a tip diameter of 50 $\mu m$, designed to minimise its influence on the flow and to avoid microbubbles sticking to the sensor.

Fig. 3(a) shows a schematic of the tank with the locations tested for the probe for a water depth of 80 cm and Fig. 3(b) shows the corresponding dissolved oxygen concentrations over time obtained for the repeats of the experiments under two operating conditions. Although the saturation concentration of dissolved oxygen varies along the water column due to hydrostatic pressure (c. 1% for 10 cm of water), it is seen that the DO concentration evolution is very similar at different locations despite small fluctuations and the resulting mass transfer coefficients are equal within $\pm 1.4\%$. Although low void fractions and small bubble sizes are investigated, the estimation of mass transfer coefficient does not depend on the location of the DO probe. In addition, the effects of hydrostatic pressure on the estimation of mass transfer coefficients have been neglected here as Petera and Ditl (2000) showed that the error caused by the pressure profile on the transfer coefficient under current conditions ($h \simeq 1m$) is less than 2%.

The dissolved oxygen concentration $C_L$ in the tank is driven by the following equation:

$$(1 - \epsilon_G)\frac{dC_L}{dt} = -k_L a(C_L - C_L^*), \tag{7}$$

where $\epsilon_G$ is the void fraction, $C_L$ the oxygen concentration in water, $C_L^*$ is the saturation concentration of oxygen in water and $k_L a$ is the volumetric mass transfer coefficient. In the experiments reported here, the void fraction is in the range 0.1–0.5% except in a few cases with Pentanol aqueous solution where it reached c. 1%. The void fraction being very low, it has been neglected in the present study to estimate mass transfer coefficients. The evolution of oxygen concentration as a function of time therefore writes:

$$C_L \simeq C_L^*\left(1 - e^{-k_L a\ t}\right). \tag{8}$$

The volumetric mass transfer coefficient $k_L a$ can be derived from the time evolution of the oxygen concentration as the slope of $-\ln\left(1 - C_L/C_L^*\right)$ against time. Fig. 4(a) and (b) show the evolution of oxygen concentration as a function of time in logarithmic and linear scales respectively for three different flow rates. It is seen that Eq. 8 describes the present experiments across the range of flow rates studied and that the mass transfer coefficient depends on the flow rate of air.

In the following, experiments have been performed in a water depth of 1.15 m unless otherwise stated and the effects of water depth on oxygen transfer are presented in Appendix A. The bubble sizes and their velocities are two key parameters to characterise oxygen transfer from bubble clouds in aqueous solutions, hence bubble sizes and velocities are reported together with oxygen transfer coefficients and efficiencies in Section 3.

*2.2. Experimental setup with wastewater*

Experiments were performed in wastewater in a $2m^3$ circular tank with a water depth of 1 m (see Fig. 5). The system comprised the wastewater from a meat factory, with a number of microorganisms and fed with raw condensate, concentrated in ammonia, that needs to be treated through a conventional nitrification process (Daigger and Littleton, 2014):

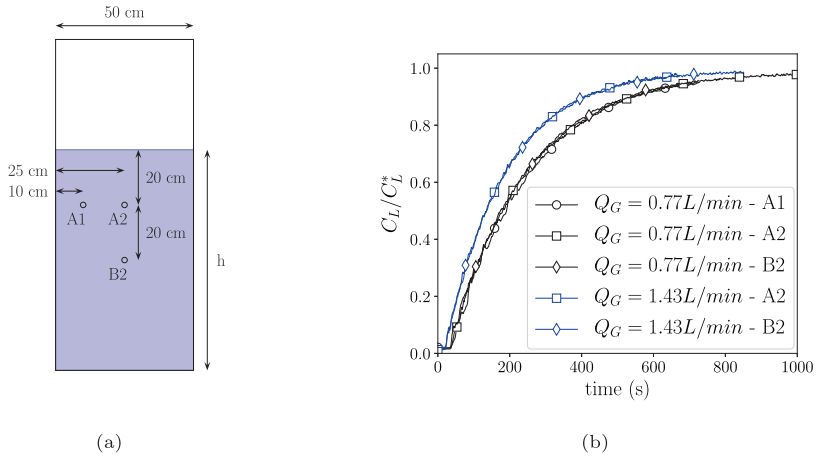


(a) (b)

**Fig. 3.** DO probe locations tested (a) and corresponding DO results as a function of time for 2 gas flows (b).

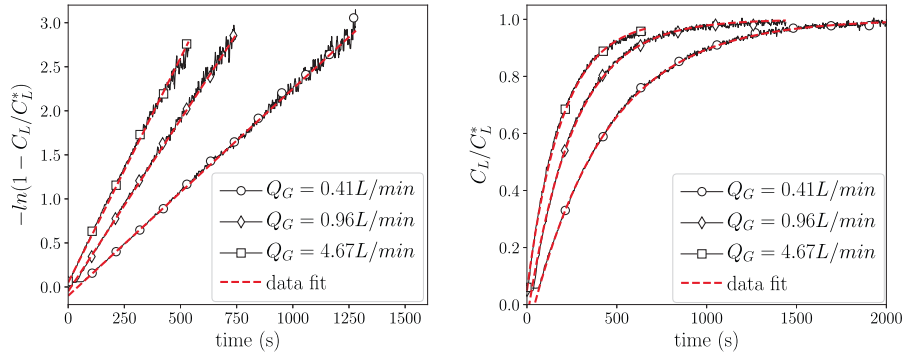


(a) (b)

**Fig. 4.** Time series of the oxygen concentration and mass transfer coefficients fitting.

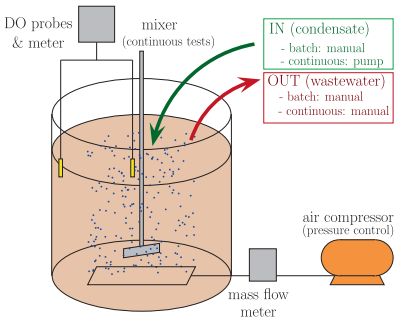


**Fig. 5.** Schematic of the rig on site for tests with wastewater.

$$NH_4^+ + 1.5\,O_2 \rightarrow NO_2^- + H_2O + 2H^+ \quad (9)$$

$$NO_2^- + 0.5\,O_2 \rightarrow NO_3^- \quad (10)$$

Some more details on the condensate and its physico-chemical properties as well as the use of hydrophobic membrane for ammonia removal from this condensate can be found in Brennan et al. (2020).

Diffusers connected to a compressor delivering clean dry air are placed at the bottom of the tank, which is filled up to 1 m depth. Two types of diffusers have been tested to deliver oxygen in wastewater: *(i)* the same ceramic diffusers as those used in the laboratory experiments, which can deliver bubbles with diameters down to c. 100$\mu m$ (see Section 3.1), and *(ii)* membrane diffusers (Europelec 250[2]), which generate bubbles with diameters bigger than 1 mm (supplier data) and which are more commonly used in industrial and municipal wastewater aeration tanks. Two DO probes (ABB ADS 430), connected to a DO meter (ABB AWT 440) for monitoring oxygen concentration, are located at the center and on the outer part of the tank, about 15 cm under the surface and the air flow is measured with a mass flow meter (SMC PFM711S-F02-B). Two modes of operation have been tested: (*i*) batch mode and (*ii*) continuous mode to mimic the plant operation.

### 2.2.1. Batch tests

In batch tests, the objective was to measure the oxygen uptake rate in order to calculate mass transfer coefficients as described in Section 2.1.4. For this purpose, 40L of wastewater were removed and 40L of raw condensate were added to the tank. When adding raw condensate, under the condition that the pH is high enough to ensure microbial activity and therefore oxygen consumption, the DO level decreases to zero in the tank. However, as nitrification takes place, pH decreases, thereby leading to a decrease in microbial activity and a rise in DO level which further affects the microbial activity. Due to this variation in activity over a day, an exponential curve cannot be fitted to the concentration change over time and the method derived from Eq. 8 to estimate the transfer coefficient $k_La$ cannot be directly applied. The evolution of the DO level in the tank can instead be re-written as:

[2] https://www.europelec.com/en/wp-content/uploads/sites/6/2019/07/Aquadisc-EN.pdf.

$$(1-\epsilon_G)\frac{dC_L}{dt} = -k_L a\left(C_L - C_L^*\right) + S(pH,T,C) \quad (11)$$

where $\epsilon_G$ is the void fraction, negligible here and $S(pH,T,C)$ is a sink term which accounts for the oxygen consumption by the micro-organisms. In addition, the microbial activity depends strongly on several factors that could not be kept constant through the tests, such as pH, temperature and DO level. As a consequence the evolution of DO over time shown in Fig. 6 does not exhibit en exponential increase as in Fig. 4 and lacks repeatability due to changes in pH and therefore in the oxidation/reduction potential and microbial activity.

Fig. 6(a) shows that the evolution of oxygen at two different locations is identical and therefore the estimation of transfer coefficient does not depend on the probe location. However, Fig. 6(b) shows that for a given flow rate of air, the increase in oxygen over time is not reproducible on different days. Fig. 7 shows the evolution of the time derivative of the DO level as a function of DO. As nitrification takes place, levels of ammonia decrease and alkalinity is consumed, thereby decreasing the pH and therefore the activity of micro-organisms. The last term on the right hand side of Eq. 11 becomes negligible and a linear trend, which is expected in the absence of sink term, is approached when the DO level reaches 5.5 to 8 mg/L. Transfer coefficients have therefore been estimated as the tangent of the rate of change of dissolved oxygen before it stabilises as shown in Fig. 7 and the coefficients obtained are reproducible within ±15%.

#### 2.2.2. Continuous tests

In the continuous tests, a flow rate of raw condensate was continuously pumped into the tank and wastewater was removed daily to keep a constant volume. The flow and removal rates were set to mimic the plant operation with a 28 days residence time of the condensate in the aeration tank. Oxygen was also continuously injected to reach a balance with DO values between 1 and 5 mg/L. A number of parameters have been monitored: DO and temperature (continuously) as well as Ammonium as Nitrogen (NH4-N), Nitrite as Nitrogen (NO2-N), Nitrate as Nitrogen (NO3-N), pH, Total Suspended Solids (TSS) and Chemical Oxygen Demand (COD) once to twice per day. Table 2 shows the average and the standard deviation of the feeding and consumption rates of NH4-N and COD for air flow rates of 8 and 16L/min over 3 and 4 weeks respectively. It is observed that both NH4-N and COD consumption rates are close to the feeding ones, *i.e.* the removal rates are above 80%, thereby showing a good activity of the micro-organisms. Those removal rates are however subject to strong fluctuations and significant deviations were observed on weeks 4 and 6. These deviations are assumed to be due to the adaptation of the living organisms to the new tank conditions: (*i*) higher DO level and oxidation/reduction potential on week 4 when changing the air flow rate and (*ii*) high pH on week 6, which lead to a decrease in micro-organism activity. In addition, the levels of NO2-N and NO3-N measured suggest that full nitrification (Eqs. 9,10) takes place and a mass balance has been achieved assuming that 1 g and 4.6 g of oxygen have been used for consuming 1 g of COD and 1 g of NH4-N respectively. The oxygen transfer efficiency for COD and NH4-N removal therefore writes:

$$OTE = \frac{\left[\left(\dot{m}^f_{COD} - \dot{m}^c_{COD}\right) + 4.6\left(\dot{m}^f_{NH4-N} - \dot{m}^c_{NH4-N}\right)\right]\Delta t}{Q_G C_G \Delta t} \times 100, \quad (12)$$

where $\dot{m}$ are the feed and consumption rates of COD and NH4-N and $C_G$ is the concentration of oxygen in air. Table 2 shows the oxygen transfer efficiencies and these results are discussed in more details in Section 3.3.

## 3. Results

### 3.1. Bubble sizes

The bubble size distributions generated by a microporous ceramic plate are studied under various operating conditions. Fig. 8 shows the volumetric bubble size distributions and the cumulative distributions obtained in tap water for different air flow rates -or superficial gas velocities-. At low superficial gas velocity, we observe narrow distributions with a peak around 500 $\mu m$. As the pressure is increased and the superficial gas velocity increases, the generated bubbles are bigger and two peaks are observed on the distributions, one around 500 $\mu m$ and another around $2mm$ and increases further as the flow rate of air increases. This second peak for flow rates $Q_G \geqslant 1.78 L/min$ is attributed to coalescence and it also results in a change in the shape of the cumulative distributions as can be seen in Fig. 8(b).

Fig. 9 shows the Sauter diameters as a function of the injection velocity or gas superficial velocity for various aqueous solutions. With tap water, a linear increase in the Sauter diameter is shown as the superficial gas velocity increases until approximately $U_G = 3mm/s$. At higher superficial velocities, as the coalescence rate is enhanced, the increase in Sauter diameter with superficial gas velocity is again linear but with much greater rate of growth. It is observed that the bubble sizes with Triton and Pentanol-3 at low concentration are slightly smaller than those obtained with tap water due to the increase in the relative effects of buoyancy over surface energy effects. However, a similar trend is observed, namely the bubble sizes increase linearly at low flow rate and a second linear trend with a higher rate of increase appears at superficial velocities about $3mm/s$, when coalescence becomes more significant. However, with increasing concentration of Pentanol-3, the bubbles are smaller than those obtained with water or low concentrations of Pentanol-3 and we do not observe a transition to the coalescence regime. The effects on the bubble cloud was also observed during the experiments where a much denser cloud was produced suggesting that bubbles no longer coalesced after injection. As a result post-processing of images where too many bubbles are overlapping was no longer possible with high concentration of Pentanol-3 but the effects of the reduced coalescence on oxygen transfer are presented in Section 3.3.

### 3.2. Bubble swarm dynamics

The bubble swarm generated and the flow obtained depends on several factors: *(i)* the bubble column aspect ratio, *(ii)* the flow rate of air (or the resulting void fraction), *(iii)* the bubble sizes and *(iv)* the fluid properties. Delnoij et al. (1997) studied the effects of the bubble column aspect ratio on the flow structure from pseudo steady state (single-cell bubbly flow and double-cell transition flow) to unsteady vortical flows. In the experiments reported in this study, the bubble swarm followed an unsteady vortical flow structure, *i.e.* with oscillating recirculation cells on the sides, for all the superficial gas velocities tested. This is in agreement with the studies of Laupsien et al. (2017) and Delnoij et al. (1997) where similar unsteady vortical structures were observed in bubble columns of aspect ratio larger than 2. Fig. 10 shows the regime observed at low flow rates with small bubbles ($d_{sa} \sim 500\mu m$) and at high flow rates ($d_{sa} \sim 2.5mm$). Both tests show similar vortical structures although it is clear that more bubbles are present in the column at low flow rate. As the rise velocity increases with bubble sizes, the residence time of small bubbles ($d_{sa} \sim 500\mu m$) is longer than that of larger bubbles ($d_{sa} \sim 2.5mm$). In addition, the Stokes number, which characterises the tendency of bubbles to follow the streamlines, is defined as $St_k = t_0 u_0 / l_0$ where $t_0$ is

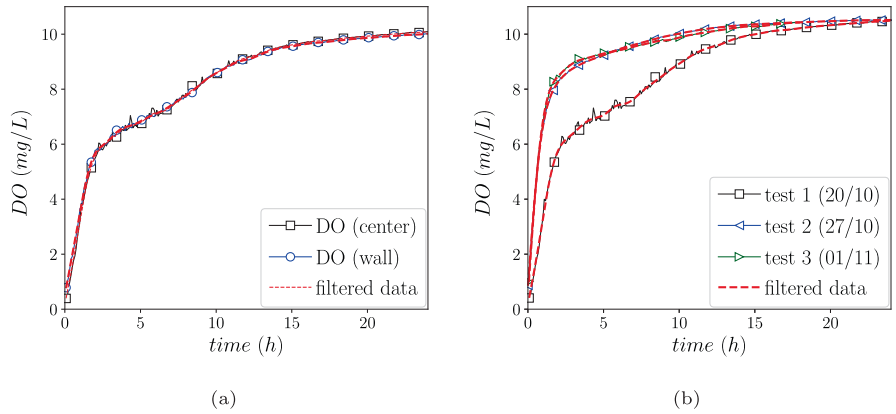


**Fig. 6.** Dissolved oxygen concentration as a function of time (a) at various locations in the tank and (b) at different dates under the same operating conditions ($Q_G = 16L/min$).

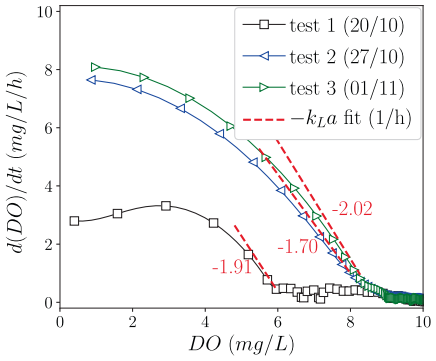


**Fig. 7.** Time derivative of the dissolved oxygen concentration as a function of dissolved oxygen concentration.

the relaxation time of the particle and $u_0$ and $l_0$ are the characteristic velocity and length of the flow respectively. The relaxation time of bubbles increases with their sizes ($\sim d_B^2$) so the residence time of microbubbles is also enhanced as their Stokes number is reduced and they tend to follow the streamlines, *i.e.* the recirculation motion that is seen in the images.

The average rise velocities of the bubbles in a number of aqueous solutions are shown in Fig. 11 as a function of the superficial gas velocity. Although the bubble sizes experience two different linear trends with the increase in the superficial gas velocity, the velocities evolve linearly in both regimes observed (without and with coalescence), as it is the case in other studies at higher void fraction (Colombet et al., 2015). Velocities of bubbles in low concentration Pentanol-3 solutions are very close to those observed in tap water with a linear increase as the superficial velocity increases. However, the velocities obtained in Triton X100 are slightly lower due to an increase in drag. Similarly to Triton X100, the bubble velocities in high concentrations Pentanol-3 aqueous solutions are slower than those in tap water and are close to those in aqueous solution of Triton X100 because the bubbles are smaller (see Fig. 9) and the interface is contaminated so the drag is increased (Takagi and Matsumoto, 2011).

### 3.3. Oxygen transfer rate

Fig. 12(a) shows the volumetric transfer coefficient as a function of the superficial gas velocity. This corresponds to the transfer rate or the inverse of a characteristic time to transfer oxygen. Three different trends can be observed for water, Triton X100 and Pentanol-3 solutions up to 0.1 $mol.m^{-3}$: *(i)* the volumetric transfer coefficient increases with the superficial gas velocity, *i.e.* the characteristic time to oxygenate water decreases, *(ii)* it stabilises and *(iii)* starts increasing again smoothly. The plateau observed ($U_G = [3; 6]\,mm/s$) corresponds to the transition to coalescence regime inferred from bubble size trends in Figs. 8 and 9. In addition, the present transfer coefficients obtained with bubbles between the micro and milli scale are higher than the results obtained with millibubbles and lower than those obtained with microbubbles in Muroyama et al. (2013). Indeed, at a given superficial gas velocity or a given volume of air injected, microbubbles provide a much greater interfacial area.

In addition to being a barrier to mass transfer (Jimenez et al., 2014; Lebrun et al., 2022), the presence of surfactants leads to a rigidification of the interface and hence, results in increased drag coefficient, reduced rise velocity and reduced coalescence (Takagi and Matsumoto, 2011). As a consequence the mass transfer properties are strongly affected by the presence of contaminants. Although the volumetric mass transfer coefficients increase as the air superficial velocity increases with all the aqueous solutions tested, two very different trends are observed:

- The volumetric mass transfer coefficients are reduced with Triton X100 as a result of interface contamination. The effects of contamination weaken as the superficial gas velocity increases, which can be explained by the increase in bubble sizes and velocities which result in a decreased capture efficiency of contaminants at the interface (Huang et al., 2012).

**Table 2**
NH4-N and COD feed, consumption and removal rates and OTE in continuous tests.

| $Q_G$ [$L/min$] | | $\dot{m}^f$ [$g/day$] | $\dot{m}^c$ [$g/day$] | removal [%] | OTE [%] |
|---|---|---|---|---|---|
| 8 | NH4-N | $52.0 \pm 2.1$ | $43.4 \pm 7.2$ | $83.6 \pm 13.0$ | $22.4 \pm 4.8$ |
| | COD | $567.5 \pm 69.1$ | $554.1 \pm 105.7$ | $98.3 \pm 13.1$ | |
| 16 | NH4-N | $52.7 \pm 1.6$ | $50.1 \pm 15.2$ | $95.9 \pm 30.1$ | $9.7 \pm 1.7$ |
| | COD | $463.2 \pm 89.3$ | $443.1 \pm 100.6$ | $97.2 \pm 19.8$ | |

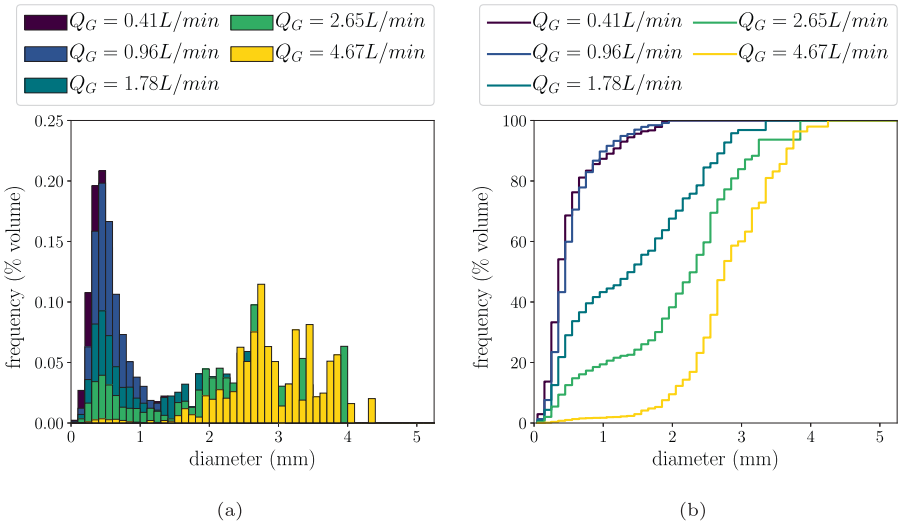


**Fig. 8.** Volumetric bubble size distributions (a) and cumulative buble size distributions (b).

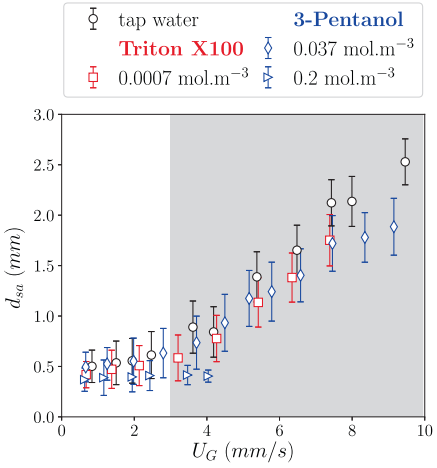


**Fig. 9.** Sauter diameter as a function of the superficial gas velocity. The grey area represents the flow rates where coalescence takes place.

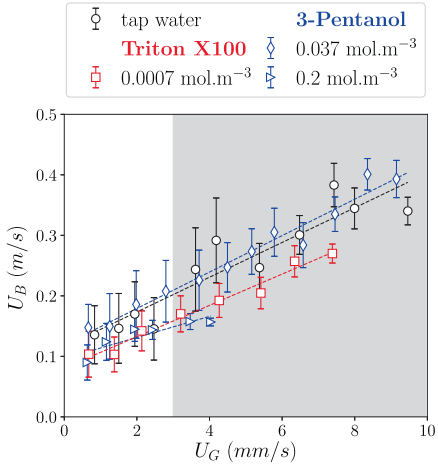


**Fig. 11.** Bubble vertical velocities as a function of the gas superficial velocity. The dashed lines show the linear fits for the different aqueous solutions. The grey area represents the coalescence regime observed in Fig. 9.

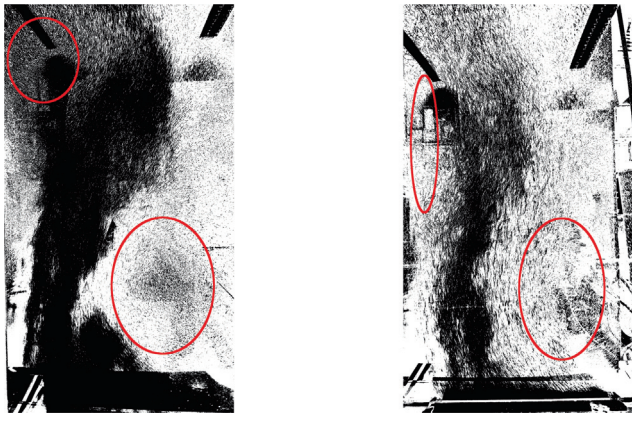

(a) $Q = 0.41L/min$ (b) $Q = 4.67L/min$

**Fig. 10.** Flow regimes observed in the bubble column with water.

- The volumetric mass transfer coefficients with Pentanol-3 are enhanced when compared with tap water. Although a surprising result as contamination is expected to reduce transfer coefficients, it was observed that coalescence is reduced when increasing the concentration in Pentanol-3 solutions. As a result, high interfacial areas are obtained at a given flow rate and the volumetric mass transfer coefficients approach the complete absorption model by Muroyama et al. (2012).

These trends are confirmed by the transfer efficiency, *i.e.* the ratio of the quantity of air transferred to the depleted liquid over a time $\Delta t$ ($k_L a C_L^* V \Delta t$) and the quantity of air injected ($Q_G C_G \Delta t$). The Oxygen Transfer Efficiency (OTE) is then written:

$$OTE = \frac{k_L a C_L^* V \Delta t}{Q_G C_G \Delta t} \times 100 = \frac{k_L a C_L^* h}{U_G C_G} \times 100, \tag{13}$$

where $V$ is the volume of the tank, $h$ is the water depth and $C_G$ is the concentration of oxygen in air. Fig. 12(b) shows the OTE obtained as a function of the operating conditions. Although three regimes were observed with the trends in transfer coefficients, the transfer efficiency is shown to decrease monotonically. From an application point of view, it should also be pointed out that the transfer efficiencies obtained at low flow rates ($U_G \leqslant 2mm/s$) with water or

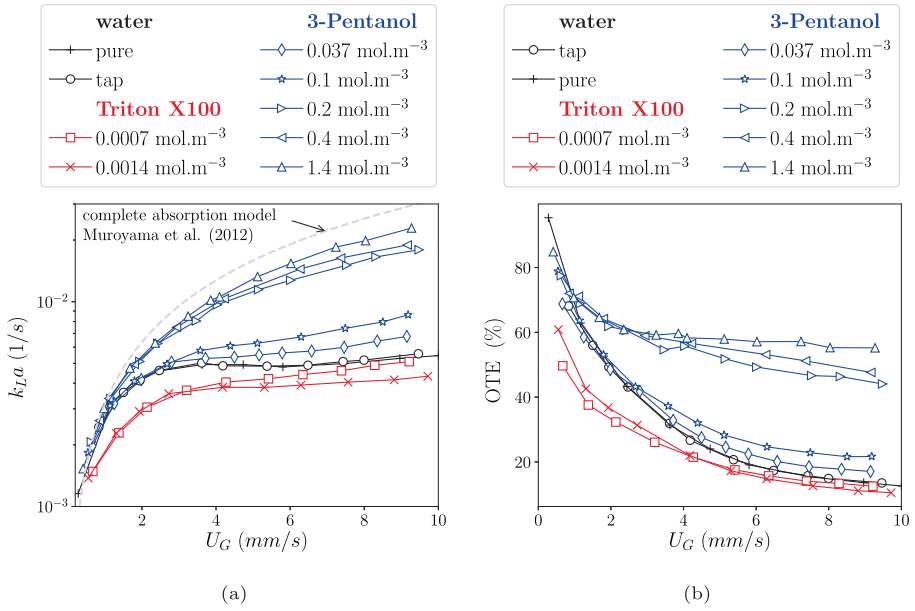


**Fig. 12.** Volumetric mass transfer coefficient (a) and oxygen transfer efficiency (b) as a function of the superficial gas velocity for various aqueous solutions.

Pentanol-3 solutions up to 0.1 $mol.m^{-3}$ and across the range of flow rates for higher concentrations of Pentanol-3 are above 50 %, which is considered to be sufficient to transfer most of the oxygen from a bubble in a 5 m deep aeration tank considering that the tests are performed with only 1 m water depth. Indeed, from a purely oxygenation efficiency perspective, microbubbles down to a few micrometers, whose generation requires high energy to break the interface are typically not justified in aeration tanks unless very fast transfer is required (Terasaka et al., 2011). In addition, these high transfer efficiencies suggest significant bubble depletion along the bubble column. The oxygen partial pressure in the bubbles decreases and as a result, the transfer driving force in Eq. 7 is reduced. The effects of bubble depletion on the estimation of mass transfer coefficients and the Sherwood number are further discussed in Appendix A and Section 3.4. The effects of contamination with Triton X100 are particularly significant at low flow rates with a decrease in transfer efficiency of c. 35% while the difference with water at high flow rates is dampened. This is in agreement with the observations of McClure et al. (2017) who found a 3-5-fold decrease in Oxygen Transfer Rate with the addition of antifoaming agents up to a critical concentration, assumed to be the threshold for the bubbles to be fully covered by a monolayer of antifoam. However, the effects of Pentanol-3 are highlighted at high flow rates where the reduced coalescence affects dominantly the specific interfacial area. The effects of surfactants on the specific interfacial areas and the transfer coefficients respectively are further analysed in Section 3.4.

The oxygen transfer efficiencies obtained in wastewater in batch and continuous tests are compared to aqueous solutions in Fig. 13. The results are reported in $OTE(\%)/m$ to account for the slight difference in water depth ($1 - 1.15m$). It should be noted that the transfer efficiency strongly depends on the average DO level in the tank. Indeed, transfer coefficients measured in batch mode corresponded to transfer efficiencies from a depleted solution while the DO levels were non zero and varied during the continuous tests. In order to compare the results, continuous tests have been converted to standard conditions, $SOTE = OTE\,(C_L^* - DO)/C_L^*$ where $C_L^*$ is the saturation concentration and $DO$ is the dissolved oxygen level in the tank during the continuous tests. It is observed that the SOTE obtained in wastewater

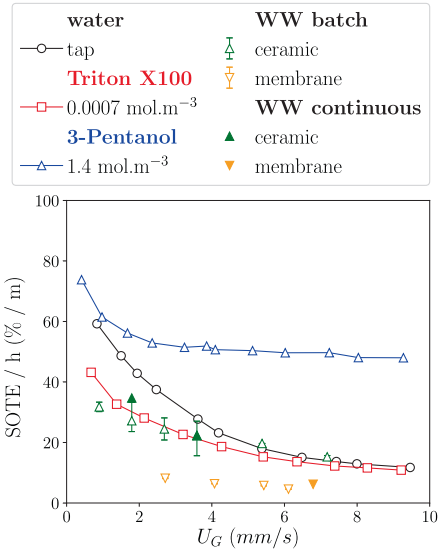


**Fig. 13.** Oxygen transfer efficiency in aqueous solutions and in wastewater.

with the ceramic diffusers are very similar to those obtained with the solution of Triton X100 with the same diffusers across the range of operating conditions tested: they are decreased by c. 40–45% when compared to transfer efficiencies in tap water at low flow rate while the diminution in SOTE from the contaminants is less significant at high flow rate. This is due to bigger size of bubbles and higher velocities, which lead to higher convection effects (Takemura and Yabe, 1998) and a decreased capture efficiency of contaminants (Huang et al., 2012). In addition, the effects of bubble sizes in wastewater are also highlighted with reporting the transfer efficiencies about 8%/m obtained with a membrane diffuser (Europelec 250 ), which generate bubbles with diameters bigger than 1 mm (according to the supplier data). The results from the membrane diffuser are used here as a reference as they are used in industrial and municipal wastewater aeration tanks and they are in agreement with the results obtained in Muroyama et al. (2013) with millimetric bubbles. With a porous ceramic plate as

the one used in the lab experiments, transfer efficiencies at high flow rates (*i.e.* with $1mm \leqslant d_{sa} \leqslant 3mm$) are about twice as high as those obtained with membrane diffusers. However, at lower flow rates, bubbles are expected to be much smaller and the difference increases, with transfer efficiencies reaching about 30–35%/m, *i.e.* about 4 times more efficient than millibubbles generated with a membrane diffuser.

### 3.4. Discussion on volumetric interfacial areas and oxygen transfer coefficients

To study in more details the effects of contaminants on mass transfer, Fig. 14 shows the two contributions to interfacial transfer, namely the specific or volumetric interfacial area $a$ and the mass transfer coefficient $k_L$, as a function of the gas superficial velocity. The splitting of the contributions $k_L$ and $a$ is made possible by the dual measurement of the oxygen concentration and the bubble sizes. It shows that the solution of Pentanol-3 at low concentration and that of Triton X100 follow the same trends as those obtained with water, i.e. the specific interfacial area increases until a superficial velocity of $3\,mm/s$ and then decreases as coalescence takes place before reaching a plateau at $7\,mm/s$. However, it is observed that the specific interfacial areas are slightly higher in contaminated solutions than they are in tap water due to the reduced surface tension and therefore the buoyancy of the bubbles overcoming the surface adhesion forces earlier in contaminated solutions during bubble formation. The specific interfacial areas observed in Pentanol-3 solutions at high concentrations are however much higher and keep increasing as the gas superficial velocity increases as a result of decreased surface tension and coalescence reduction. Finally, when isolating the contributions of specific interfacial areas and transfer coefficients it shows that the transfer coefficients obtained in Pentanol-3 solution at low concentration are similar to those obtained with water while the coefficients in higher concentration solutions and Triton X100 are reduced, which is consistent with the effects of those surfactants on the drag coefficient (Takagi and Matsumoto, 2011).

Finally, the effects of surfactants on mass transfer are characterised through the competition between the convective and diffusive mass transport thanks to the Sherwood number $Sh = k_L^* d_{sa}/D$, where $D$ is the mass diffusivity of oxygen in liquid. Due to the small concentrations of surfactants, the diffusion coefficient of water was used. Lebrun et al. (2022) calculated the diffusion coefficient in aqueous solutions of Triton X100 and showed no or negligible effects of this surfactant on the mass diffusivity. Also, as discussed in Appendix A, the significant bubble depletion at low flow rates and the resulting overestimation of the mass transfer driving force in Eq. 7 leads to an underestimation of the ability of the bubbles to transfer oxygen and thus the Sherwood number. We therefore use the corrected values $k_L^*$ as derived in Appendix A to estimate the Sherwood number.

Fig. 15 shows the Sherwood number as a function of the Reynolds number ($Re = Ud_{sa}/\nu$ with $\nu$ the kinematic viscosity of water) for the Pentanol-3 and Triton X100 aqueous solutions considered in this study. As suggested by Colombet et al. (2015) who measured mass transfer of millimetric bubbles in water, single-bubble correlations for the interfacial mass transfer provide accurate predictions for mass transfer in bubble swarm and the liquid agitation does not have significant effects. Takemura and Yabe (1998) measured the dissolution of millimetric bubbles in water and proposed the following correlation:

$$Sh^{TY} = \frac{2}{\sqrt{\pi}}\left(1 - \frac{2}{3\left(1 + 0.09Re^{2/3}\right)^{3/4}}\right)^{1/2}\left(2.5 + Pe^{1/2}\right). \tag{14}$$

This expression was validated experimentally and numerically (Figueroa-Espinoza and Legendre, 2010) in the case of mobile interfaces. For the lower Peclet numbers ($Pe = ReSc = Ud_{sa}/D$)) where it has been observed that interface contamination plays a key role in mass transfer, we retain the expression obtained by Frössling (1938) for rigid interfaces:

$$Sh^F = 0.6Re^{1/2}Sc^{1/3}. \tag{15}$$

It is also worth mentioning the work of Rosso et al. (2006) who quantified the contamination effects on mass transfer with the introduction of an interface contamination number $Ro = c_B t_B D_{SAA}^3/\sigma d_B^3$ where $c_B$ represents the bulk surfactant concentration, $t_B$ the bubble age, $D_{SAA}$ the surfactant bulk diffusivity, $\sigma$ the surface tension and $d_B$ the bubble diameter. The empirical fitting of the Sherwood number from their experiments resulted in the following expression:

$$Sh^R = \frac{0.382Pe^{1/3}}{1 + \log\left[1 + 10^{19}Ro\right]}. \tag{16}$$

However, this correlation underestimates the Sherwood number obtained in the present study, even when considering Ro = 0, *i.e.* without contamination. These discrepancies could be explained by the fact that in Rosso et al. (2006), the lower Peclet numbers were about $5 \times 10^5$ while the range of Peclet numbers investigated here is in the range $10^4 \leqslant Pe \leqslant 4 \times 10^5$.

We observe that the Sherwood number in water and in low concentration of Pentanol-3 ($0.037mol.m^{-3} - \Gamma/\Gamma_{max} \simeq 0.002$) in the lowest range of Reynolds number ($Re \leqslant 100$) is slightly higher than the one of a solid sphere (Frössling, 1938) while in the range $100 \leqslant Re \leqslant 1000$, the Sherwood number approaches the correlation from Takemura and Yabe (1998) obtained with clean interfaces. The Sherwood numbers in contaminated solutions decreases as the interface coverage increases at low Reynolds numbers ($Re \leqslant 200$). The Sherwood numbers obtained at low Reynolds numbers with high concentration of Pentanol-3 ($0.2mol.m^{-3} - \Gamma/\Gamma_{max} \simeq 0.06$) agree well with the results of a rigid sphere while the Sherwood numbers obtained with Triton X100 ($\Gamma/\Gamma_{max} \simeq 0.43$) are lower than the predictions from Frössling (1938) correlation. This is in agreement with the recent results of Jimenez et al. (2014) and Lebrun et al. (2022), suggesting that the oxygen transfer is not only affected by the change in dynamics due to the contamination of the interface but the surfactants also act as a barrier to mass transfer. However, the results also transition to the Sherwood numbers for clean interfaces as the Reynolds number increases. These results also suggest that contamination effects are enhanced at low Reynolds numbers, *i.e.* when the bubbles sizes and velocities are the smallest. This is attributed to two main mechanisms: *(i)* surfactants are advected to the rear of the bubbles as they rise, even more so when inertia dominates diffusion effects, *i.e.* as the bubbles sizes and velocities increase; and *(ii)* as the Peclet number increases, the boundary layer thickness in front of the bubbles decreases and oxygen transfer primarily takes place at the front cap (Figueroa-Espinoza and Legendre, 2010). As a result, even if the bubble rear cap is contaminated, the effects on mass transfer become negligible. The following empirical expression based on the results at low Reynolds number and the asymptotic behaviour of the clean interface trends at high Reynolds number shows a good agreement with the experimental results across the range of Reynolds numbers tested:

$$Sh = \frac{\alpha Sh^F + \beta Re^2 Sh^{TY}}{1 + \beta Re^2} \tag{17}$$

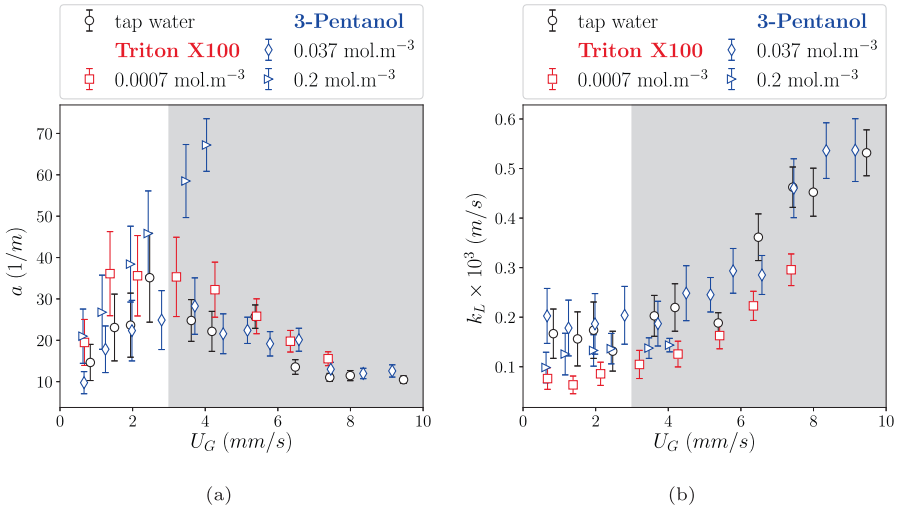


**Fig. 14.** Volumetric interfacial area (a) and mass transfer coefficient (b) as a function of the superficial gas velocity for various aqueous solutions.

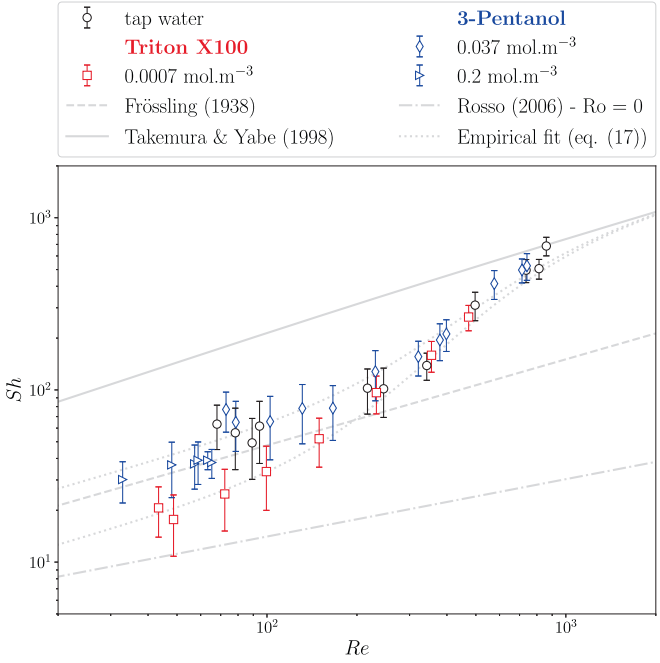


**Fig. 15.** Sherwood number as a function of the Reynolds number for Pentanol-3 and Triton X100 aqueous solutions.

with $\beta = 2.5 \times 10^{-6}$ and $\alpha = [1.25; 1.25; 1; 0.6]$ for water, Pentanol-3 at $0.037\,mol.m^{-3}$, Pentanol-3 at $0.2\,mol.m^{-3}$ and Triton X100 at $0.0007\,mol.m^{-3}$ respectively. This simple model should however be tested in a wider range of operating conditions (Re, Sc, surfactants) and the empirical coefficients should be correlated to the physico-chemical properties of the surfactants and the interfacial coverage dynamics.

## 4. Conclusion

Dual measurement of *(i)* the oxygen concentration with an optical probe and *(ii)* the bubble sizes with visualisation techniques have been performed over a wide range of operating conditions. This allowed the detailed investigation of the role of the interfacial area and the mass transfer coefficient on oxygen transfer efficiency in bubble swarms between micro and millibubbles.

- The diminution in OTE as the flow rate increases was shown and the good performance of porous ceramic plates at low flow rate, where microbubbles ($d_{sa} \simeq 500\mu m$) are generated is highlighted for both clean water and wastewater.
- A methodology to compare laboratory experiments with industrial wastewater with microbiological activity is presented for two modes of operation.
- The relevance of laboratory tests with Triton X100 to study oxygen transfer in wastewater is of particular interest. This is of main importance as this shows the potential to further study oxygen transfer relevant to wastewater conditions under a well controlled laboratory framework. It would be valuable to confirm or extend those observations to other operating conditions and with other surfactants and wastewater.
- Contamination of the interface with both Pentanol-3 and Triton X100 is shown to reduce coalescence, *i.e.* increase the specific interfacial area, and decrease the mass transfer coefficient. Although the volumetric mass transfer coefficients increase with Pentanol-3 concentration, the present dual experiments show that this increase is due to the increase in volumetric interfacial area while the mass transfer coefficient $k_L$ actually decreases with Pentanol-3 concentration.
- The effects of contamination are shown to decrease as the bubble sizes increase. All the aqueous solutions show a transition from a modified Frössling correlation ($Sh = \alpha Sh^F$) to the Sherwood number predicted by Takemura and Yabe (1998) for clean interfaces as the Reynolds number increases ($200 \leqslant Re \leqslant 1000$). An expression was proposed and still needs to be confirmed with more surfactant solutions and the parameters fitted empirically here should ultimately be correlated to the properties of the surfactants. Further investigation is still required to better understand the combined effects of contamination on mass transfer and the role of hydrodynamics as the interface solidifies on one hand and the mass-transfer inhibition on the other hand.

## CRediT authorship contribution statement

**Thomas Abadie:** Conceptualization, Methodology, Validation, Formal analysis, Investigation, Resources, Data curation, Visualization, Writing – Original Draft, Writing – Review & Editing. **Sultan M. al Ma Awali:** Formal analysis, Investigation. **Brian Brennan:** Formal analysis, Investigation. **Ciprian Briciu-Burghina:** Formal analysis. **Mohammad Tajparast:** Conceptualization, Formal analy-

sis. **Thayse Marques Passos** Formal analysis. **John Durkan:** Resources. **Linda Holland:** Funding acquisition. **Jenny Lawler:** Funding acquisition. **Kieran Nolan:** Funding acquisition. **Brid Quilty:** Conceptualization, Funding acquisition. **Lorna Fitzsimons:** Funding acquisition. **Fiona Regan:** Supervision, Funding acquisition. **Yan Delauré:** Conceptualization, Methodology, Writing – Review & Editing, Supervision, Funding acquisition.

## Declaration of Competing Interest

The authors declare that they have no known competing financial interests or personal relationships that could have appeared to influence the work reported in this paper.

## Acknowledgements

This research was co-funded by the European Regional Development Fund (ERDF) and ABP Food Group, Ireland, under Ireland's European Structural and Investment Funds Programmes 2014–2020 and Enterprise Ireland Innovation Partnership Programme. The project code associated with this research grant is IP2015 0415. The authors would like to acknowledge ABP Food Group for the support and providing access to their installations. TA also acknowledges Michael May (DCU) for the support provided while building the experimental facilities as well as the contributions of Thomas Dixneuf and Cedric Le Page (visiting students) for their help in building and running some experiments.

## Appendix A. Effects of water depth and bubble depletion on oxygen transfer

The effects of water depth on oxygen transfer have been investigated for depths varying from 0.6 m to 1.15 m. Increasing the water depth provides a longer residence time to the bubble and for practical applications, it is essential that this depth but also other tank geometry features be taken into account when chosing the bubble diffusers and the bubble swarms they generate. Fig. A.16(a) shows a decrease in transfer coefficient as the water depth increases while the transfer efficiency increases as the depth and the residence time of the bubbles increase (Fig. A.16(b)). However, the increase with water depth is not linear as shown in Fig. A.17. The transfer efficiencies normalised by the water depths are equal for h = 1 m and 1.15 m but then increase with decreasing water depth. This suggests that the depletion of the bubbles as they rise leads to a decreased efficiency in the higher part of a tank (Talvy et al., 2007) or that a significant part of the transfer takes place in the vicinity of the plate.

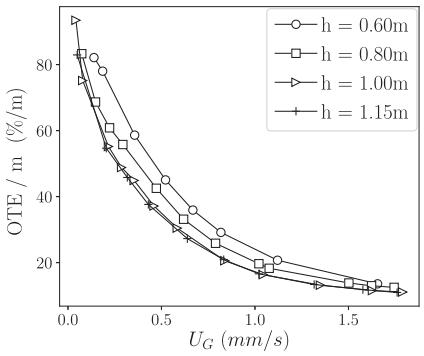


**Fig. A.17.** Oxygen transfer efficicncy normalised with the water depth as a function of the superficial gas velocity.

To estimate the effects of depletion, we consider the evolution of oxygen concentration in the bubbles as they rise together with the evolution of dissolved oxygen concentration in the liquid:

$$\frac{dC_G}{dt} = -\frac{k_L^* a}{\epsilon_G}\left(C_{L,interface} - C_L\right), \tag{A.1}$$

$$\frac{dC_L}{dt} = -k_L a(C_{L,sat} - C_L)\ , \tag{A.2}$$

where $k_L^* a$ is the transfer coefficient accounting for the actual oxygen transfer driving force $(C_{L,interface} - C_L)$ while the mass transfer coefficient in Eq. (A.2) is an "apparent" transfer coefficient. Note that this approach considers that the volume of the bubbles do not vary significantly as they only contain 20% of oxygen. The time for the bubbles to rise along the water column $h/U_B \simeq 3 - 10s$ while the characteristic time for mass transfer in the liquid is $1/k_L a \simeq 200 - 1000s$. Considering that *(i)* the concentration on the liquid side of the interface is $C_{L,interface} = mC_G$ where $m$ is the concentration jump corresponding to the oxygen solubility; and *(ii)* that while the bubbles rise in the liquid over a time $\Delta t^{rise} \sim h/U_B$, the bulk concentration can be considered constant; Eq. A.1 can easily be integrated:

$$C_G(t) = \frac{C_L(t_0)}{m} + \frac{C_{L,sat} - C_L(t_0)}{m}\exp\left(-\frac{k_L^* am}{\epsilon_G}(t - t_0)\right), \tag{A.3}$$

where $t_0$ is the time of injection of the bubbles. A first order approximation of the change in $C_L$ between the injection and when the bubbles reach the surface (*i.e.* over $\Delta t^{rise} = h/U_B$) is:

$$C_L(t_0 + h/U_B) - C_L(t_0) = -k_L a(C_{L,sat} - C_L(t_0))\frac{h}{U_B}. \tag{A.4}$$

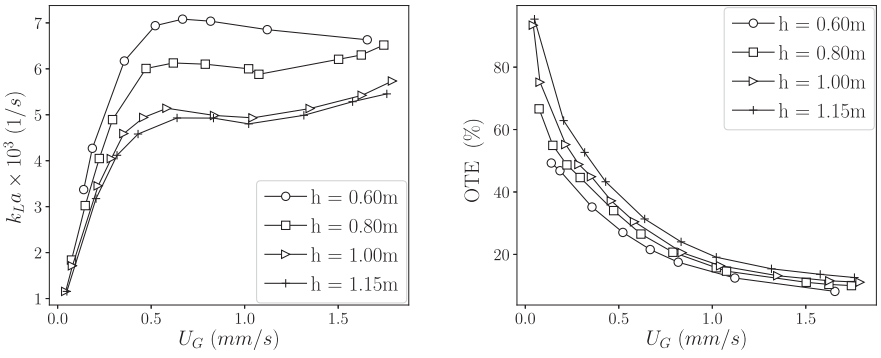


(a) (b)

**Fig. A.16.** Volumetric mass transfer coefficient (a) and oxygen transfer efficiency (b) as a function of the superficial gas velocity for various water depths.

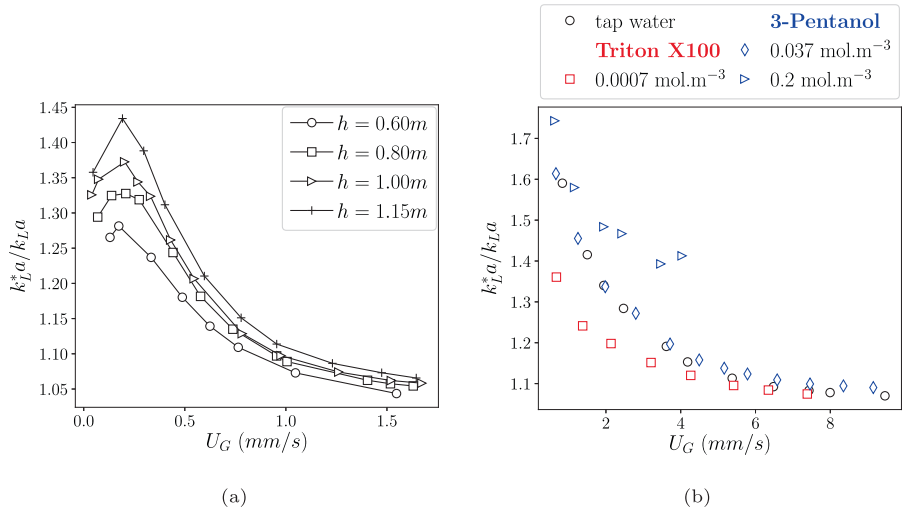


(a) (b)

**Fig. A.18.** Ratio of corrected to apparent mass transfer coefficients as a function of the gas injection rate in (a) pure water with varying water depth and (b) aqueous solutions at a fixed water column height ($h = 1.15m$).

And considering that $dC_L/dt \simeq \epsilon_G dC_G/dt$, we have:

$$-k_L a(C_{L,sat} - C_L(t_0))\frac{h}{U_B} = \epsilon_G(C_G(t_0 + h/U_B) - C_G(t_0)) \quad (A.5)$$

$$= \frac{\epsilon_G}{m}(C_{L,sat} - C_L(t_0))\left[\exp\left(-\frac{k_L^* am}{\epsilon_G}\frac{h}{U_B}\right) - 1\right]. \quad (A.6)$$

We can then deduce a relation between the apparent mass transfer coefficient measured from the evolution of dissolved oxygen to the actual mass transfer coefficient accounting for the bubble depletion and the decrease in mass transfer driving force:

$$k_L^* a = -\frac{U_B \epsilon_G}{hm}\left[ln\left(-\frac{k_L ahm}{U_B \epsilon_G}\right) + 1\right]. \quad (A.7)$$

It is seen that if the bubble is not being depleted (large $U_B$ or small $h$ for instance), the corrected coefficient tends towards the measured apparent one. Fig. A.18(a)-(b) show the ratio of the corrected mass transfer coefficient to the measured one with different water depths and with various aqueous solutions respectively. We can see that the effects of depletion are highlighted at low injection rate (small bubbles and low void fraction) and they are emphasized as the water depth increases. The effects of depletion are also enhanced when working with concentrated 3-Pentanol solutions as coalescence is reduced while the effects of depletion are reduced with Triton X100 as oxygen transfer efficiencies are reduced.

## References


Agarwal, A., Ng, W.J., Liu, Y., 2011. Principle and applications of microbubble and nanobubble technology for water treatment. Chemosphere 84, 1175–1180.

Brennan, B., Briciu-Burghina, C., Hickey, S., Abadie, T., al Ma Awali, S.M., Delaure, Y., Durkan, J., Holland, L., Quilty, B., Tajparast, M., Pulit, C., Fitzsimons, L., Nolan, K., Regan, F., Lawler, J., 2020. Pilot Scale Study: First Demonstration of Hydrophobic Membranes for the Removal of Ammonia Molecules from Rendering Condensate Wastewater. Int. J. Mol. Sci. 21, 3914.

Brenner, H., 1963. Forced convection heat and mass transfer at small Péclet numbers from a particle of arbitrary shape. Chem. Eng. Sci. 18, 109–122.

Brittle, S., Desai, P., Ng, W.C., Dunbar, A., Howell, R., Tesar, V., Zimmerman, W.B., 2015. Minimising microbubble size through oscillation frequency control. Chem. Eng. Res. Des. 104, 357–366.

Calgaroto, S., Azevedo, A., Rubio, J., 2015. Flotation of quartz particles assisted by nanobubbles. Int. J. Miner. Process. 137, 64–70.

Calgaroto, S., Wilberg, K., Rubio, J., 2014. On the nanobubbles interfacial properties and future applications in flotation. Miner. Eng. 60, 33–40.

Colombet, D., Legendre, D., Cockx, A., Guiraud, P., 2013. Mass or heat transfer inside a spherical gas bubble at low to moderate Reynolds number. Int. J. Heat Mass Transf. 67, 1096–1105.

Colombet, D., Legendre, D., Cockx, A., Guiraud, P., Risso, F., Daniel, C., Galinat, S., 2011. Experimental study of mass transfer in a dense bubble swarm. Chem. Eng. Sci. 66, 3432–3440.

Colombet, D., Legendre, D., Risso, F., Cockx, A., Guiraud, P., 2015. Dynamics and mass transfer of rising bubbles in a homogenous swarm at large gas volume fraction. J. Fluid Mech. 763, 254–285.

Daigger, G.T., Littleton, H.X., 2014. Simultaneous Biological Nutrient Removal: A State-of-the-Art Review. Water Environ. Res. 86, 245–257.

Delnoij, E., Kuipers, J., van Swaaij, W., 1997. Dynamic simulation of gas-liquid two-phase flow: effect of column aspect ratio on the flow structure. Chem. Eng. Sci. 52, 3759–3772.

Durán, C., Fayolle, Y., Pechaud, Y., Cockx, A., Gillot, S., 2016. Impact of suspended solids on the activated sludge non-newtonian behaviour and on oxygen transfer in a bubble column. Chem. Eng. Sci. 141, 154–165.

Etchepare, R., Oliveira, H., Nicknig, M., Azevedo, A., Rubio, J., 2017. Nanobubbles: Generation using a multiphase pump, properties and features in flotation. Miner. Eng. 112, 19–26.

Figueroa-Espinoza, B., Legendre, D., 2010. Mass or heat transfer from spheroidal gas bubbles rising through a stationary liquid. Chem. Eng. Sci. 65, 6296–6309.

Frössling, N., 1938. Über die verdunstung fallenden tropfen (evaporation of falling drop). Gerlands Beitage zur Geophysik 52, 170–216.

Garcia-Ochoa, F., Gomez, E., 2009. Bioreactor scale-up and oxygen transfer rate in microbial processes: An overview. Biotechnol. Adv. 27, 153–176.

Germain, E., Nelles, F., Drews, A., Pearce, P., Kraume, M., Reid, E., Judd, S., Stephenson, T., 2007. Biomass effects on oxygen transfer in membrane bioreactors. Water Res. 41, 1038–1044.

Hebrard, G., Zeng, J., Loubiere, K., 2009. Effect of surfactants on liquid side mass transfer coefficients: A new insight. Chem. Eng. J. 148, 132–138.

Huang, Z., Legendre, D., Guiraud, P., 2012. Effect of interface contamination on particle–bubble collision. Chem. Eng. Sci. 68, 1–18.

Jimenez, M., Dietrich, N., Grace, J.R., Hébrard, G., 2014. Oxygen mass transfer and hydrodynamic behaviour in wastewater: Determination of local impact of surfactants by visualization techniques. Water Res. 58, 111–121.

Kawahara, A., Sadatomi, M., Matsuyama, F., Matsuura, H., Tominaga, M., Noguchi, M., 2009. Prediction of micro-bubble dissolution characteristics in water and seawater. Exp. Thermal Fluid Sci. 33, 883–894.

Khadre, M.A., Yousef, A.E., Kim, J.-G., 2001. Microbiological Aspects of Ozone Applications in Food: A Review. J. Food Sci. 66, 1242–1252.

Khuntia, S., Majumder, S.K., Ghosh, P., 2012. Microbubble-aided water and wastewater purification: a review. Rev. Chem. Eng. 28.

Laupsien, D., Cockx, A., Line, A., 2017. Bubble Plume Oscillations in Viscous Fluids. Chem. Eng. Technol. 40, 1484–1493.

Lebrun, G., Benaissa, S., Le Men, C., Pimienta, V., Hébrard, G., Dietrich, N., 2022. Effect of surfactant lengths on gas-liquid oxygen mass transfer from a single rising bubble. Chem. Eng. Sci. 247, 117102.

Li, P., Tsuge, H., 2006. Water Treatment by Induced Air Flotation Using Microbubbles. J. Chem. Eng. Japan 39, 896–903.

Liu, C., Chen, X.-X., Zhang, J., Zhou, H.-Z., Zhang, L., Guo, Y.-K., 2018. Advanced treatment of bio-treated coal chemical wastewater by a novel combination of microbubble catalytic ozonation and biological process. Sep. Purif. Technol. 197, 295–301.

Matsumoto, Y., Uda, T., Takagi, S., 2006. The effect of surfactant on rising bubbles. In: S. Balachandar, A. Prosperetti (eds.), Proceedings of the IUTAM Symposium on Computational Multiphase Flow, Springer, pp. 311–321.
McClure, D.D., Deligny, J., Kavanagh, J.M., Fletcher, D.F., Barton, G.W., 2014. Impact of Surfactant Chemistry on Bubble Column Systems. Chemi. Eng. Technol. 37, 652–658.
McClure, D.D., Lamy, M., Black, L., Kavanagh, J.M., Barton, G.W., 2017. An experimental investigation into the behaviour of antifoaming agents. Chem. Eng. Sci. 160, 269–274.
Muroyama, K., Imai, K., Oka, Y., Hayashi, J., 2013. Mass transfer properties in a bubble column associated with micro-bubble dispersions. Chem. Eng. Sci. 100, 464–473.
Muroyama, K., Oka, Y., Fujiki, R., 2012. Transport Properties of Micro-Bubbles in a Bubble Column. J. Chem. Eng. Japan 45, 666–671.
Parmar, R., Majumder, S.K., 2013. Microbubble generation and microbubble-aided transport process intensification—A state-of-the-art report. Chem. Eng. Process. 64, 79–97.
Petera, K., Ditl, P., 2000. Effect of pressure profile on evaluation of volumetric mass transfer coefficient in kLa bioreactors. Biochem. Eng. J. 5, 23–27.
Rodríguez-Rodríguez, J., Sevilla, A., Martínez-Bazán, C., Gordillo, J.M., 2015. Generation of Microbubbles with Applications to Industry and Medicine. Annu. Rev. Fluid Mech. 47, 405–429.
Rodrigues, R.T., Rubio, J., 2007. DAF–dissolved air flotation: Potential applications in the mining and mineral processing industry. Int. J. Miner. Process. 82, 1–13.
Roghair, I., Van Sint Annaland, M., Kuipers, J., 2016. An improved Front-Tracking technique for the simulation of mass transfer in dense bubbly flows. Chem. Eng. Sci. 152, 351–369.
Rosso, D., Huo, D.L., Stenstrom, M.K., 2006. Effects of interfacial surfactant contamination on bubble gas transfer. Chem. Eng. Sci. 61, 5500–5514.
Rosso, D., Stenstrom, M.K., 2006. Surfactant effects on a-factors in aeration systems. Water Res. 40, 1397–1404.
Rubio, J., Souza, M., Smith, R., 2002. Overview of flotation as a wastewater treatment technique. Miner. Eng. 15, 139–155.
Sardeing, R., Painmanakul, P., Hébrard, G., 2006. Effect of surfactants on liquid-side mass transfer coefficients in gas–liquid systems: A first step to modeling. Chem. Eng. Sci. 61, 6249–6260.
Takagi, S., Matsumoto, Y., 2011. Surfactant Effects on Bubble Motion and Bubbly Flows. Annu. Rev. Fluid Mech. 43, 615–636.
Takahashi, M., 2005. ? Potential of Microbubbles in Aqueous Solutions: Electrical Properties of the Gas-Water Interface. J. Phys. Chem. B 109, 21858–21864.
Takemura, F., 2005. Adsorption of surfactants onto the surface of a spherical rising bubble and its effect on the terminal velocity of the bubble. Phys. Fluids 17, 048104.
Takemura, F., Yabe, A., 1998. Gas dissolution process of spherical rising gas bubbles. Chem. Eng. Sci. 53, 2691–2699.
Talvy, S., Cockx, A., Liné, A., 2007. Modeling of oxygen mass transfer in a gas–liquid airlift reactor. AIChE J. 53, 316–326.
Tavassoli, H., Peters, E.A.J.F., Kuipers, J.A.M., 2017. Direct numerical simulation of non-isothermal flow through dense bidisperse random arrays of spheres. Powder Technol. 314, 291–298.
Terasaka, K., Hirabayashi, A., Nishino, T., Fujioka, S., Kobayashi, D., 2011. Development of microbubble aerator for waste water treatment using aerobic activated sludge. Chem. Eng. Sci. 66, 3172–3179.
Tesar, V., 2013. Microbubble smallness limited by conjunctions. Chem. Eng. J. 231, 526–536.
Tesar, V., 2014. Mechanisms of fluidic microbubble generation Part II: Suppressing the conjunctions. Chem. Eng. Sci. 116, 849–856.
Tesar, V., Peszynski, K., 2014. Water oxygenation by fluidic microbubble generator. EPJ Web of Conferences 67, 02116.
Tsuge, H., 2014. Micro- and Nanobubbles: Fundamentals and Applications. Jenny Stanford Publishing.
Vasconcelos, J.M.T., Rodrigues, J.M.L., Orvalho, S.C.P., Alves, S.S., Mendes, R.L., Reis, A., 2003. Effect of contaminants on mass transfer coefficients in bubble column and airlift contactors. Chem. Eng. Sci. 58, 1431–1440.
Walz, M.-M., Werner, J., Ekholm, V., Prisle, N.L., Öhrwall, G., Björneholm, O., 2016. Alcohols at the aqueous surface: chain length and isomer effects. Phys. Chem. Chem. Phys. 18, 6648–6656.
Weisstein, E.W., 2003. Oblate Spheroid.
Wu, Z., Chen, H., Dong, Y., Mao, H., Sun, J., Chen, S., Craig, V.S.J., Hu, J., 2008. Cleaning using nanobubbles: defouling by electrochemical generation of bubbles. J Colloid Interface Sci 328, 10–14.
Zhang, W.-H., Zhang, J., Zhao, B., Zhu, P., 2015. Microbubble Size Distribution Measurement in a DAF System. Ind. Eng. Chem. Res. 54, 5179–5183.
Zimmerman, W.B., Tesar, V., Bandulasena, H.H., 2011. Towards energy efficient nanobubble generation with fluidic oscillation. Curr. Opin. Colloid Interface Sci. 16, 350–356.